Plasma proteome association and catalytic activity of stealth polymer-grafted iron oxide nanoparticles

Miaoyi Wang,[†a] Ghizal Siddiqui,[‡a] Ove J. R. Gustafsson,[¶] Aleksandr Käkinen,[†] Ibrahim Javed,[†] Nicolas H. Voelcker,[‡, ¶] Darren J. Creek,[‡] Pu Chun Ke[†] and Thomas P. Davis[†,§*]*

[†] ARC Centre of Excellence in Convergent Bio-Nano Science and Technology, Monash Institute of Pharmaceutical Sciences, Monash University, 381 Royal Parade, Parkville, VIC 3052, Australia

[‡] Monash Institute of Pharmaceutical Sciences, Monash University, 381 Royal Parade, Parkville, VIC 3052, Australia

[¶] ARC Centre of Excellence in Convergent Bio-Nano Science and Technology, Future Industries Institute, University of South Australia, University Boulevard, Mawson Lakes, SA 5095, Australia

[§] Department of Chemistry, University of Warwick, Gibbet Hill, Coventry, CV4 7AL, United Kingdom

[a] The authors contributed equally to the work.

KEYWORDS: Iron oxide nanoparticles, PEG, PC, plasma proteins, proteomics, abundance

ABSTRACT

Polyethylene glycol (PEG) has been widely used as an antifouling and stealth polymer in surface engineering and nanomedicine. However, recent research has revealed adverse effects of bioaccumulation and immunogenicity following the administration of PEG, prompting this proteomic examination of the plasma protein coronae association with superparamagnetic iron oxide nanoparticles (IONPs) grafted with brushed PEG (bPEG) and an alternative, brushed phosphorylcholine (bPC). Using label-free quantitation by liquid chromatography tandem-mass spectrometry we determined protein abundances for the *in vitro* hard coronae of bare, bPC- and bPEG-grafted IONPs in human plasma. We show unique protein compositions in the plasma coronae of each IONP, including enrichment of coagulation factors and immunogenic complement proteins with bPEG, and enhanced binding of apolipoproteins with bPC. Functional analysis revealed that plasma protein coronae elevated the horseradish peroxidase-like activities of the bPC- and bPEG-IONPs by ~twofold, an effect likely mediated by the diverse composition and physicochemical properties of the polymers as well as their associated plasma proteins. Taken together, these observations support the rational design of stealth polymers based on a quantitative understanding of the interplay between IONPs and the plasma proteome, and should prove beneficial for the development of materials for nanomedicine, biosensing and catalysis.

INTRODUCTION

When introduced to a biological fluid such as blood, nanoparticles (NPs) spontaneously adsorb a layer of proteins, saccharides and lipids to render a "corona".[1] The formation of the corona is driven by electrostatic and hydrophobic interactions, hydrogen bonding, as well as van der Waals forces, and also depends upon the physicochemical properties of the NPs (size, shape, surface charge, and hydrophobicity).[2] A "soft" corona is initially formed by proteins of high abundance and is eventually displaced by proteins of high affinity, as ascribed by the Vroman effect.[3] The protein corona reduces the surface energy of the NPs while often enhancing their suspendability and biocompatibility.[2,4] Importantly, the protein corona underpins the biological identity and fate of the NPs, in stark contrast to that of the pristine NPs. It is this acquired biological identity that further dictates cell interactions,[5,6] uptake,[7] biodistribution and clearance of the NPs *in vivo*.[8-10]

Polyethylene glycol (PEG) has been widely used as a grafting and antifouling agent in biotechnology, surface science, packaging and chemical engineering.[11] PEG is completely miscible in water and assumes an expandable conformation or "entropic spring" in the aqueous phase to resist protein and ligand adsorption.[12] Despite its prevalent use, the perception that PEG is a perfect solution to antifouling and "stealth" applications has been increasingly challenged.[13-17] For example, PEG binds lysozyme through hydrophobic interactions and PEGylated polystyrene NPs exhibit affinity for apolipoproteins A-I and E, as well as complement proteins that are actively involved in immunogenicity.[15-17] In addition, PEG is not biodegradable and thus chronic administration of PEGylated drugs leads to accumulation of the polymer *in vivo*. Moreover, anti-PEG antibodies have been found in healthy subjects and in patients treated with PEG-conjugated agents, while severe hypersensitivity reactions have also been reported for some patients.[18] These findings highlight the need for developing alternative strategies to PEGylation for biotechnological and biomedical applications.

Phosphorylcholine (PC) is a structural component of phosphatidylcholine and sphingomyelin. Like PEG, PC has been employed as an antifouling agent for the treatment of surfaces and nanostructures against protein adsorption.[19-22] Recently, we have demonstrated a facile synthesis scheme of grafting superparamagnetic iron oxide nanoparticles (IONPs) with brushed poly(2-(methacryloyloxy)ethyl phosphorylcholine) (poly(MPC)) via a phosphonic acid linker.[23] The structural details of these IONPs, grafted with either brushed PEG (bPEG) or PC (bPC), were examined in the presence of human serum albumin (HSA), the most abundant protein in the blood plasma. Compared to bPEG, bPC conferred comparable or superior IONP suspendability, stability, cell adsorption, cell uptake and protein antifouling.[24] These advantages were attributed to the high polarity and biomimetic nature of the zwitterionic PC, compared to the synthetic and hydrophilic PEG. The cylindrical morphology of PC brushes further entailed a higher grafting density than the spherical PEG brushes.[24]

The *in vivo* circulation half-life and intended function of IONPs grafted with polymers or polymer brushes depend upon the composition of the protein corona. Proteomics can quantify changes in the composition and abundance of the protein coronae for different NPs. Indeed, label-free quantitation (LFQ) by liquid chromatography coupled to mass spectrometry (LC-MS/MS) is often the method of choice as it allows comparisons of relative abundance across multiple NP coronae.[25,26] Using this approach it has recently been shown that the LC-MS/MS corona fingerprints for a library of gold and silver NPs can be used to predict cell association, and that these fingerprints appear to be unique to both the surface chemistry and NP core material.[5] Human plasma coronae have already been studied by LC-MS/MS approaches for dextran-coated IONPs, indicating that dextran does not completely cover the particle surface,[27] and that the corona formed has a minimal impact on macrophage uptake and subsequent particle clearance.[7,27]

In addition to the broad applications in magnetic resonance imaging and nanomedicine,[28-32] IONPs have recently been found to act as horseradish peroxidase (HRP) mimetics, opening the door to a

range of chemical sensing and diagnostic applications.[33,34] It is logical to expect that the presence of a plasma protein corona would interfere and modulate the intended functions of the IONPs, a hypothesis tested in this study.

To facilitate the applications of IONPs in nanomedicine and theranostics [35-37] and to establish a database concerning PEG and PC as major stealth polymers, here we present a proteomic characterisation of IONPs grafted with bPEG and bPC (scheme see Figure 1a) following exposure to human plasma. The global quantitative protein data presented provides an in-depth evaluation of bPC as an alternative to bPEG and complements the previously observed superior physical characteristics of bPC grafting. To achieve this, we applied LFQ by LC-MS/MS to determine protein abundances for the hard coronae of bare, bPC- and bPEG-grafted IONPs in plasma. This allowed for determination of both the identities and abundance of plasma opsonins bound to these IONPs. We demonstrated that the three IONPs surfaces were associated with unique protein subsets, that unique biological processes could be impacted by these coronae, and that bPC is a viable alternative to bPEG for surface grafting of IONPs.

MATERIALS AND METHODS

Zeta potential

The three types of IONPs were synthesized as described in reference 23. The zeta potentials of the IONPs were determined using a dynamic light scattering device (Zetasizer Nano Nano-ZS, Malvern Instruments) at room temperature (Figure 1b).

Transmission electron microscopy

5 μL aliquot of IONPs (bare IONPs, bPEG-IONPs and bPC-IONPs) at 0.1 mg/mL concentration was pipetted onto glow discharged (15 s) 400 mesh copper grids (Formvar film, ProSciTech) and allowed for 60 s of adsorption. Excess samples were then drawn off using filter paper and the grids were washed twice using 10 μL Milli-Q water, with excess drawn off. The grids were then air-dried as needed. Imaging was performed on a Tecnai G2 F20 Transmission Electron Microscope (FEI, Eindhoven, The Netherlands) operating at a voltage of 200 kV. Images were recorded using an UltraScan 1000 P 2k CCD camera (Gatan, California, USA) and Gatand Digital Micrograph 3.9.5 software. The TEM imaging was done three times to ensure reproducibility. The sizes of the three types of IONPs were determined to be ~15-20 nm in diameter (Figure 1c).

Collection and processing of human plasma

Blood was collected from a healthy human donor after obtaining informed consent in accordance with the University of Melbourne Human ethics approval 1443420 and the Australian National Health and Medical Research Council Statement on Ethical Conduct in Human Research. Blood was drawn by venipuncture into Vacuette® (Greiner Bio-One) collection tubes containing sodium heparin and inverted 5 times. Cells were removed from blood by centrifugation (950 *g*, 12 min, low brake). Centrifugation was repeated on the supernatant and the resulting plasma was transferred to fresh tubes and stored at 4˚C until use.

Corona formation and isolation

Bare, bPEG and bPC grafted IONPs (5 mg/mL) in 0.01 M PBS were mixed with blood plasma to make the final concentration of each type of IONPs to 0.5 mg/mL in 1 mL suspension. The IONP/plasma mixtures were incubated in a shaker at 37 °C for 24 h and then loaded onto a 0.7 M sucrose cushion solution and mixed well. Sample suspensions were centrifuged at 16,300 *g* for 15 min at room temperature to isolate IONP-protein 'hard' corona complexes from the remaining plasma.

The supernatant was completely removed and the IONP-protein corona pellets were washed three times with 0.01 M freshly made PBS. Following washes, 50 µL of 5% β-mercaptoethanol (Sigma-Aldrich™) in 4× reducing loading dye was added into each IONP sample and the mixture was incubated at 95 °C for 5 min. IONPs were pelleted by centrifugation for 3 min at 21,100 *g* and 4 °C and the supernatants (20 µL) of each sample were resolved using a precast gel (Mini-PROTEAN® TGX™, Bio-Rad Laboratories). The protein gel was run in reducing buffer (25 mM Tris, 192 mM glycine, 0.1% SDS) for 5 min at 200 V/0.04 A/8 W. The protein gel was incubated in Instant Blue stain (Expedion Ltd) for 30 min on a shaker to fix and visualize the proteins. Milli-Q water was used to destain the gel for 1 h (fresh Milli-Q water every 20 min).

In-gel proteolytic digestion

Following staining, the entire region where the sample had been resolved was cut from the gel using sterile scalpels and Petri dishes. The protein gel piece was diced into square cubes (~2 mm^2) and transferred into 1.5 mL tubes. The gel pieces were further destained using 1.5 mL of destaining buffer (100 mM ammonium bicarbonate, Thermo Fisher) (ABC) for 5 s (vortex mixed). Supernatants were then removed and 1.5 mL of destaining buffer 2 (50% of 100 mM ABC and 50% of acetonitrile (MERCK) (ACN) was added and incubated for 20 min on a roller. The supernatant was removed and the destaining step 2 was repeated with fresh destaining buffer 2. The proteins were then reduced and alkylated using tris(2-carboxyethyl)phosphine hydrochloride (TCEP) (Sigma-Aldrich™) (5 mM in 100 mM ABC) and iodoacetamide (Sigma-Aldrich™) (11 mM in 100 mM ABC) incubated at 95 °C for 5 min. Supernatant was removed and the gel pieces were washed once with 500 µL of destaining buffer 2 (vortex mixed), washed twice with 1.5 mL ACN for 15 min and dried in a vacuum centrifuge (Labconco). Reduced and alkylated proteins were then digested using 2 µg sequencing grade Trypsin (Promega) for 16 h in an automated vortex at 37 °C. Following digestion, 150 µL of extraction buffer (50% ACN, 5% formic acid (Fisher chemical) (F.A) in 100 mM ABC) was added to each sample

(~300 µL total volume in each tube) and vortex mixed. The supernatants were collected and the above step was repeated and supernatants collected and combined with the first extraction step. Finally, 150 µL of ACN was added to each sample and incubated on a rotor for 10 min until gel pieces were completely dehydrated. This final supernatant was collected, pooled with the other extract supernatants and the gel pieces were discarded. Supernatants from each gel band were completely dried using a vacuum centrifuge. Dried peptide samples were then resuspended in 20 µL of 2% ACN and 0.1% F A in Milli-Q water, sonicated and mixed using an automated vortex to ensure complete resuspension. The final samples were centrifuged at 21,100 g at 4 °C for 3 min and collected into LC-MS vials.

Plasma control sample preparation

Human plasma (15 µL) was incubated with 1% trichloroacetic acid (Sigma-Aldrich) in isopropanol at a ratio of 1:10 (plasma to organic solvent) to effectively remove ~90% of HSA.[38] HSA is a highly abundant protein within human plasma that has several unwanted effects on LC-MS/MS analysis. This includes interference with the MS signal of low abundant proteins and limiting sample loading capability on the LC-MS/MS system due to saturation of the mass spectrometric signal from high abundance peptides following digestion.[38] Following partial HSA removal, the sample was vortexed and centrifuged at 1500 *g* at 4 °C for 5 min. Following centrifugation, the supernatant was discarded and the pellet was washed with 200 µL of methanol. The sample was vortexed and centrifuged at 600 *g* at 4 °C for 3 min. The supernatant was removed and the pellet was resuspended in 200 µL of 100 mM 4-(2-hydroxyethyl)-1-piperazineethanesulfonic acid) (HEPES) pH 8.1. The proteins were reduced and alkylated using TCEP (5 mM in 100 mM ABC) and iodoacetamide (11 mM in 100 mM ABC) incubated at 95 °C for 5 min. Reduced and alkylated protein sample was then digested for 16 h using 2 µg sequencing grade trypsin, and the peptide sample was subjected to desalting using in-house

generated StageTips as described previously.[39] The sample was then dried and resuspended in 20 µL of 2% (v/v) ACN and 0.1% (v/v) FA for LC-MS/MS analysis.

LC-MS/MS and label-free quantitation

LC-MS/MS was carried out using nano-LC coupled to a Q-Exactive™ Hybrid Quadrupole-Orbitrap Mass Spectrometer (ThermoFisher®), as described previously.[40] For label-free proteomics analysis, the LC gradient was set to 65 min using a gradient that reached 25% of ACN after 20 min, then 35% after 35 min, 45% after 49 min, 50% after 51 min, and 90% after 57 min.

Raw files were processed using MaxQuant software (version 1.5.1.2),[41] which incorporated the Andromeda search engine.[42] Proteins were identified by searching a protein sequence database containing *Homo sapiens* annotated proteins (Downloaded from Uniprot) concatenated with reversed copies of all sequences and supplemented with frequently observed contaminants (porcine trypsin and human keratin). Analysis was performed with maximum missed-cut value set to two. The following features were used in all searches: (i) fixed cysteine carbamidomethylation, (ii) variable methionine oxidation (iii) precursor mass tolerance of 10 ppm, (iv) MS/MS tolerance of 0.5 Da (v) maximum false discovery rates (FDRs) of 0.01 both on peptide and protein levels (vi) minimum required peptide length was 6 amino acids and maximum charge was 6 (vii) maximum PEP was 1 (viii) proteins with at least two peptides (thereof one uniquely assignable to the respective protein group) were considered as reliably identified.[41] The outputs from MaxQuant were then filtered to remove known contaminants such as trypsin, keratin and reverse sequences. Label-free quantification was conducted as previously described for the identification of interacting proteins.[43]

Protein hit filtering methods and significance

Experiments were conducted in triplicates to ensure reproducibility of data. Only proteins detected in at least two out of three experiments (LFQ intensity > 0) were taken for analysis. LFQ intensity was

used to approximate the relative protein abundance between different types of IONPs (Figures 3, S5-10, Tables 3, S1, S2), while intensity was used to represent the protein abundance for each type of IONPs individually (Figures 2b, S1-4, Table 1). Student's t-test was performed to test the significance of differences observed across three independent replicates and p-values < 0.05 were considered as significant. For the abundance ratio calculation and analysis, only those proteins with a p-value < 0.05 were considered significant and included in further analysis.

Protein informatics and network annotation

Uniprot *H. sapiens* proteome fasta file was downloaded (UP000005640_9606.fasta from *uniprot.org/downloads*) for export of protein sequences. R (Supplementary Information) was employed for extraction of sequences from the fasta file, as well as grand average of hydropathy (GRAVY), isoelectric point (pI) and molecular weight (MW) calculations. Missing gene names were manually updated using uniprot prior to plotting of Ln transformed LFQ intensity (plasma) or mean LFQ intensity (bPC, bPEG). R studio version 1.0.136 running R version 3.3.3 (2017-03-06) and the libraries seqinr_3.3-3, alakazam_0.2.5, ggplot2_2.2.1 and sqldf_0.4-10. See the Supplementary Information for the complete R code. Plots produced were either exported to InkScape (inkscape.org) for formatting, or used directly as R exported .tiff files converted to .png.

Protein uniprot IDs were used for online network analysis with STRING (v10, string-DB.org/).[44] A whole genome background was assumed. Database and experimentally determined interaction sources were mined using a medium confidence interaction score (0.4), without adding additional possible interactors. Network annotations (red highlighting) were used to highlight enriched gene ontology (GO) terms.

HRP-like activity

After separation of hard corona complexes of IONPs with HSA and blood plasma, the IONPs were diluted in reaction buffer (0.2 M NaAc, pH 3.5) to a concentration of 0.5 mg/mL. The HRP-like activity was determined in a 96-well microplate in quadruplicate with 100 µL of working volume consisting of 5 mM H_2O_2, 10 mM of pyrogallol as chromogenic HRP substrate and 0.125 mg/mL of IONPs in reaction buffer. Absorbance was recorded at 40 °C at 420 nm after every 60 s up to 11 min to monitor color changes as indicative of HRP-like activity. The activities of all samples were compared with each other by one-way analysis of variance (ANOVA) followed by tukey's test. P value less than 0.05 was considered as significant.

RESULTS

To achieve a quantitative comparison of protein coronae on IONPs grafted with bPC and bPEG, we used a modified version of a published protocol for label-free quantitative LC-MS/MS proteomics which is suited for IONPs.[45] The aim was to identify both the composition and any specific protein enrichment trends within the formed human plasma protein coronae. A total of 263 proteins were identified in a plasma control sample. Although there are more than 2,000 proteins present in the whole plasma proteome,[46] the remainder of the plasma proteins were below our detection limit.

Coronae summary

A total of 123 coronal proteins were confidently detected in at least 2 out of 3 biological replicates and were considered for further analysis (See below, *Protein hit filtering methods and significance*). (Figure 2). Approximately half (65) of the coronal proteins were associated with all three types of IONPs (Figure 2a; see supplementary Excel file for detail). However, the relative abundance for a number of proteins was markedly different for each IONP type (Figure 2b, Tables 3, S1 & S2). Out of

the overall 123 proteins detected, 13, 8 and 9 proteins were found to be uniquely associated with bare, bPEG and bPC coated IONPs, respectively (Table 2).

The ten most abundant proteins as well as the plasma control are listed in Table 1 for each type of the IONPs. The protein lists are similar, but there are key differences in abundance across the IONPs. HSA - the most abundant protein in human plasma (~40 mg/mL) - is also the most abundant in the protein coronae for both bare and bPEG-IONPs. However, HSA only ranks as the third most abundant for bPC-IONPs, after Ig heavy constant mu (*IGHM*) and apolipoprotein B-100 (*APOB*). Ig heavy constant gamma 1 (*IGHG1*) and complement C3 (*C3*) are among the top ten most abundant proteins for the coronae of all three IONP types as well as the plasma control (Table 1).

No relationship was observed between corona enrichment and either GRAVY index or pI. Considering the detected intensities of proteins enriched on bPC IONPs (Figures S1 and S2) and in raw plasma (Figures S3 and S4), both sets of total proteins share similar GRAVY index and pI distributions. Plotting log normalised intensity (mean intensity in Figures S1/S2) against GRAVY and pI indicates that majority of detected proteins have GRAVY values ranging from 0.1 to -1.0 and, as a group, exhibit a bimodal pI distribution, with one centred at ~ pI 6 and another within pI 8-9.

The unique corona proteins, identified for each type of IONPs, are listed in Table 2. A total of 13 proteins - Ig kappa variable 1D-33, alpha-1-antichymotrypsin, moesin, sulfhydryl oxidase 1, complement component C8 alpha chain, secreted phosphoprotein 24, properdin, beta-2-glycoprotein 1, complement C1r subcomponent, coagulation factor X, Ig gamma-2 chain C region, complement C1s subcomponent and serum amyloid P-component - were found to uniquely associate with bare IONPs. bPC-IONPs were uniquely associated with cholesteryl ester transfer protein, apolipoprotein C-II, protein disulfide-isomerase A3, phospholipid transfer protein, angiotensinogen, Ig kappa chain V-I region EU, integrin beta, Ig J chain and apolipoprotein C-I. Finally, 8 proteins were uniquely

associated with bPEG-IONPs, including pleckstrin, coagulation factor XIII A chain, 14-3-3 protein zeta/delta, fermitin family homolog 3, CD5 antigen-like, Ig heavy variable 3-72, haptoglobin and selenoprotein P (Table 2).

Specific enrichment of proteins in grafted-IONP coronae, as compared to bare IONPs

To highlight differences in inter-corona abundance, the mean fold difference was calculated by taking the average of the three independent quantitative experiments. We chose 0.5 and 2.0 fold difference as the thresholds for comparing relative protein abundance between the coronae formed on each two types of IONPs (bare IONPs versus bPEG-IONPs, bare IONPs versus bPC-IONPs, or bPEG-IONPs versus bPC-IONPs). A supplementary Excel file with mean fold differences for all proteins is provided, including those with fold differences between 0.5 and 2.0 which are not comprehensively discussed in this paper.

Seven proteins were found to have greater associations with bPC-IONPs than bare IONPs. Apolipoprotein(a) showed the biggest difference in fold differences – it was significantly less abundant for bare IONPs than for bPC-IONPs, with a fold difference of 0.07 ± 0.04 (Table S2). Conversely, 17 proteins were found to be more enriched in bare IONPs corona, with Kininogen-1 being the most abundant protein associated with bare IONPs, compared to bPC-IONPs (Table S2). When comparing bare and bPEG-coated IONPs, only hemoglobin subunit beta had less association with bare IONPs, with a fold change of 0.41 ± 0.26 (Table S1). Three protein species exhibited greater associations with bare IONPs than bPEG-IONPs, including Ig gamma-1 chain C region, complement factor B, and apolipoprotein(a).

Specific enrichment of proteins in bPC IONP coronae relative to bPEG

Six protein species were found to have less association with bPEG than bPC (Table 3) while 17 protein species were found to be more associated with bPEG (Table S6). Those which also exhibited a

total intensity proportion greater than 1% are labelled with an asterisk in Figure 2. The natural log (Ln) mean abundance ratios for the 62 proteins quantified across both bPC and bPEG (bPC:bPEG) are presented in Figure 3. The point size for the scatter plot represents the calculated GRAVY index (Figure 3a), MW (Figure 3b) and pI (Figure S5). The original mean ratio plots (no log transform) are provided in Figures S6 and S7 (zoom). The sum of these data indicated a significant split in the type, number and abundance of proteins enriched on these IONPs. At the extremes is the largest decrease in abundance for coagulation factor XI (*F11*) with a bPC:bPEG ratio of 0.11 ± 0.07 (Table 3). In sharp contrast, the largest abundance increases are observed for three types of apolipoproteins (apolipoprotein L1 [*APOL1*], B-100 [*APOB*] and apolipoprotein(a) [*LPA*]), with apolipoprotein(a) exhibiting a ~42-fold more enrichment in bPC-IONPs than bPEG-IONPs (Table 3).

General trends in the physicochemical properties of the IONP-associated protein species are observed when compared to the normalized ratios. bPEG proteins exhibited a range of GRAVY indices, in the range of 0 to -1 (Figure S8). With the exception of apolipoprotein(a), the few bPC enriched proteins exhibited GRAVY indices within the range of -0.2 to 0.5. bPC enriched proteins also exhibited pIs less than 7, while bPEG proteins are spread across the pI range of 5-9 (Figure S9). Figures 3b and S10 highlight the two proteins with the highest bPC:bPEG abundance ratio (*APOB/LPA*), both of which are larger than 500 kDa.

Figure 4 displays a protein network and gene ontology (GO) analysis using the STRING online resource.[44] The full set of matchable proteins (55/62) are included in the network, with bPC:bPEG ratios below 0.5 outlined in orange and ratios above 2.0 outlined in blue. The full color network map is provided in Figure S11. Protein network and GO analysis demonstrate that the apolipoproteins (*LPA*, *APOL1* and *APOB*) and haptoglobin related protein (*HPR*) naturally cluster together in the network, as known components of high-density lipoproteins (HDL). Furthermore, 23 of the 55 proteins in Figure 4 were assigned to the Kyoto Encyclopedia of Genes and Genomes (KEGG)

complement and coagulation cascades pathway. A closer examination of the proteins overrepresented in bPEG coronae (16 matched to STRING database) reveals that the GO biological process (BP) terms for blood coagulation (Figure S12a) and negative regulation of blood coagulation (Figure S12c) are enriched in bPEG coronae, as is the KEGG pathway for complement and coagulation cascades (Figure S12b).

HRP-like activity for IONPs in the presence and absence of coronae

An HRP assay was performed to explore the bio-activity modulation effect of the protein coronae associated with the IONPs. In addition to plasma proteins, IONPs were treated with HSA, the major protein in plasma, to differentiate the modulation imparted by HSA alone and in conjunction with other plasma proteins. In contrast to the IONPs in protein-free aqueous solution, all three IONPs coated by plasma proteins, and bPEG-IONPs coated by HSA, significantly ($p < 0.05$) increased the HRP-like activity (Figure 5). While comparing within the group, among HSA coated IONPs, bPEG-IONPs showed higher HRP-like activity ($p < 0.05$) than bPC- and bare IONPS. In contrast, among the plasma-coated IONPs, bPEG-IONPs were significantly less active ($p < 0.05$) than bPC and bare IONPs. Dynamic light scattering was employed to correlate this differential activity with the thickness and surface charge of the IONPs coated with HSA and plasma proteins (Figure 1b). Bare, bPEG and bPC coated IONPs, when incubated with HSA or plasma proteins, displayed corona-dependent surface charges and hydrodynamic sizes. Except for bPC-IONPs, coating with HSA resulted in decreased surface charge and increased hydrodynamic size for bare IONPs and bPEG-IONPs, but did not significantly ($p > 0.05$) alter the hydrodynamic size of bPC-IONPs, in accordance with the proteomic analysis of corona components (Table 1) suggesting an unfavorable interaction between bPC and HSA.

DISCUSSIONS AND CONCLUSION

A holistic evaluation of the *in vivo* suitability of a NP system requires compositional information on its protein corona. Specifically, it is of interest to determine if surface chemistry can be modified to induce either "stealth" or improved biocompatibility: both of these aims are as a function of manipulating corona composition and therefore biological identity. By applying label-free LC-MS/MS to the corona of IONPs, we were able to highlight key differences in corona composition which accompany the grafting of both bPEG and bPC, two major antifouling polymers for NPs.

Our approach to identify protein corona composition and protein affinity for NPs is more relevant than Western blotting, in that human plasma is a highly complex physiological environment consisting of more than 2,000 different proteins with various concentrations.[46] Therefore, it is necessary to consider all the protein-protein interactions and exchanges as a whole rather than isolating a few types of proteins and analyzing their affinities for NPs separately. In our method, a range of low abundant proteins can be obtained and accurately quantified whereas only selected proteins can be analyzed by Western blot.[45] In this study we have identified a total of 123 proteins. One limitation of the study is that only 'hard' corona could be identified, due to the rapid exchange of proteins in the 'soft' corona and the difficulty of isolating this protein layer from NPs. Similar to other studies, it is also clear that the compositions observed did not exactly mirror plasma and that many lower abundance proteins were significantly enriched in the IONP coronae.[7]

In order to identify trends for the protein species, we further plotted all the proteins from Table S5 and Table S6 according to their GRAVY, MW and pI. It was found that proteins that had weaker association with bPC-IONPs tended to have small MW, whereas proteins that exhibited stronger association with bPC-IONPs can possess large MW (Figure S10). bPEG and bPC-IONPs bound both acidic and basic proteins. This finding is reasonable as both bPEG and bPC-IONPs have relatively

neutral zeta potential in aqueous solution (Figure S2), thus surface charge is not the main driving force to determine protein corona.

It is also interesting to note that bPC-IONPs have a very high affinity for apolipoproteins, which are the proteins involved in lipid and cholesterol transport and metabolism, as evidenced in Table 3 and Figure S2. In addition, many of the unique proteins bound to bPC IONPs in Table 2 are involved in lipid transport and metabolism. This finding is reasonable considering the native identity of PC as a naturally occurring head group of phosphatidylcholine and sphingomyelin in the outer membrane of blood cells. When we compared bare and bPC-IONPs as well as bPEG- and bPC-IONPs, complement system proteins were enriched for both bare (complement C3, complement C1q subcomponent subunit A, B and C, complement C4-A, complement factor H and complement component C9) and bPEG-IONPs (complement factor B, complement component C9, complement C1q subcomponent subunit B and C as well as complement component C8 beta chain), as compared to bPC-IONPs. This could imply a shorter half-life in the circulation for bare and bPEG-IONPs, as the adsorption of complement proteins on NPs could induce phagocytosis.[47] It is worth noting that apart from supporting immune response, complement activation is also responsible for allergic reactions and anaphylaxis.[48] However, Ig kappa constant and Ig heavy constant mu, two proteins involved in immunogenesis, were found to be associated more with bPC-IONPs than bare and bPEG-IONPs. Furthermore, coagulation factor XI was more enriched by ~tenfold with bPEG-IONPs than bPC-IONPs (Table 3), suggesting less risk of clotting associated with the latter.

In the literature, it has been reported that PEG and PC coatings effectively reduced the quantity of proteins associated with silicon wafer surfaces corona using a Western blot method.[20] There have been studies reporting that PEGylated NPs are not able to completely avoid protein adsorption, and the proteins are likely to reside inside the PEG layer of NPs.[49] In addition, the reduced cell uptake rendered by PEGylation is undesirable for delivering cancer therapies. Thus, zwitterionic surfaces can

be promising alternatives.[49] As expected, our study indicates that neither bPEG nor bPC coating of IONPs was able to prevent protein corona formation, and a number of proteins were found to be associated with all three types of IONPs, albeit with different abundance distributions. Although the antifouling capacity of PEGylation is widely acknowledged, and supported by our previous molecular dynamics simulations and thermogravimetric analysis measurement,[24] only four corona proteins were found significantly different in abundance between bare and bPEG-grafted IONPs when thresholds of 0.5 and 2.0 were used (most of the proteins have a mean fold difference between 0.5 and 2.0, supplementary excel file). The antifouling effect of bPEG coatings on IONPs was thus limited (Table S1). However, bPC-IONPs protein coronae demonstrated more obvious differences to bare and bPEG-grafted IONPs. Specifically, less proteins were enriched in bPC coronae (Tables 3 and S2).

Our previous molecular dynamics simulations and thermogravimetric analysis measurement showed that bare IONPs possessed a higher affinity for HSA than bPEG-IONPs or bPC-IONPs, owing to the antifouling properties of bPEG and bPC.[24] In the present study, we observed that bPEG-IONPs were associated with HSA comparably to bare IONPs after 24 h of incubation. This could be due to the Vroman effect,[3] where HSA of the highest abundance was partially replaced by plasma proteins of higher affinity for the IONP core. Therefore, in order to better understand the corona proteome in a complex biological environment, it is necessary to study plasma proteins as a whole, and take into consideration of protein-protein interactions and exchanges rather than only examining the affinity of a single type of protein.

The bare IONPs displayed more aggregation than bPEG-IONPs and bPC-IONPs, while the latter two were comparable in hydrodynamic size (Figure 1b) and suspendability up to 3 days.[23] Such differences in NP aggregation may have implications for their cellular interactions through the "conditioning" process whereby cells deplete and secrete biomolecules upon exposure to NPs.[50] The grafting density for bPEG-IONPs and bPC-IONPs was 0.77 and 1.08 polymer/nm^2, respectively, to

ensure comparable molecular weights of the two types of brushed polymers per IONP.[23] The grafting densities of bPEG-IONPs and bPC-IONPs fall within the 'intermediate-high' (cluster C) and 'high' (cluster D) categorized by Walkey *et al*. for gold NPs grafted with linear PEG.[51] We noted, for example, human serum albumin [*ALB*], Ig heavy constant mu [*IGHM*], kininogen-1 [*KNG1*] and Ig kappa constant [*IGKC*], the proteins of high abundance in the LC-MS/MS study using cell culture media (with 10% fetal bovine serum) by Walkey *et al*. were also featured in our top-15 abundant corona proteins for bPEG-IONPs exposed to human plasma proteins.

Apart from their clinical application as imaging contrast agents, the catalytic capacity of IONPs is an interesting characteristic that remains to be fully exploited from a diagnostic and bioimaging perspective. The surface ferrous atoms of IONPs are considered pivotal in the HRP-like activity. However, this behavior is influenced by the balance between surface charge and the thickness of the corona on magnetic NPs.[34] A protein coat on the NP surface modulates interaction with its pharmacological receptors, bio-macromolecules and enzyme substrates. There is thus a post-opsonisation impact on the biological fate of IONPs *in vivo*. Increased HRP-like activity in H_2O_2 sensing was achieved by IONP electrodes coated with haemoglobin.[52] Similarly, plasma proteins possess an affinity for small phenolic compounds, such as pyrogallol in this study, via different functional groups, conformations and protein electronegativities.[53] The different HRP-like activities in Figure 5 may originate from the combined effect of IONPs and the different surface charge, thickness and composition of the protein coronae. For example, HSA coating enlarged the distances between surface ferrous atoms and the HRP substrate for both bPEG and bare IONPs, more so than bPC-IONPs. In the case of plasma proteins, the three most opsonized proteins on bare, bPC- and bPEG-IONPs differed as follows: vitronectin for bare and bPEG-IONPs, and IgM heavy chain C and apolipoproteins B100 for bPC-IONPs. Future efforts for establishing structure-function relationships

between IONP-specific protein coronae and their entailed HRP-like activities should prove beneficial for the development of stealth NPs for nanomedicine, biosensing and catalysis.

Supporting Information

Supporting Information is available from the Wiley Online Library or from the author.

ACKNOWLEDGMENT

This work was supported by ARC Project CE140100036 (Davis). Davis is thankful for the award of an Australian Laureate Fellowship from the ARC. The authors thank Dr. Thomas Blin for providing the iron oxide nanoparticles, ABK from Melbourne University for donating blood and Joshua Glass for purifying the blood and obtaining plasma.

FIGURES

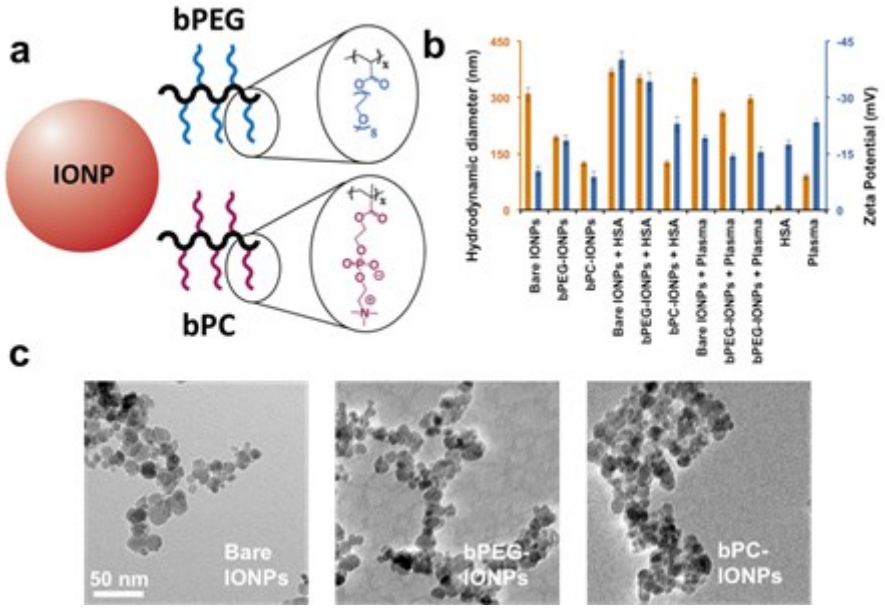

Figure 1. (a) Schemes of IONPs grafted with bPEG and bPC. (b) Hydrodynamic sizes and zeta potentials of bare, bPEG- and bPC-IONPs in aqueous solutions and with HSA and plasma proteins. (c) TEM images of bare, bPEG- and bPC-IONPs.

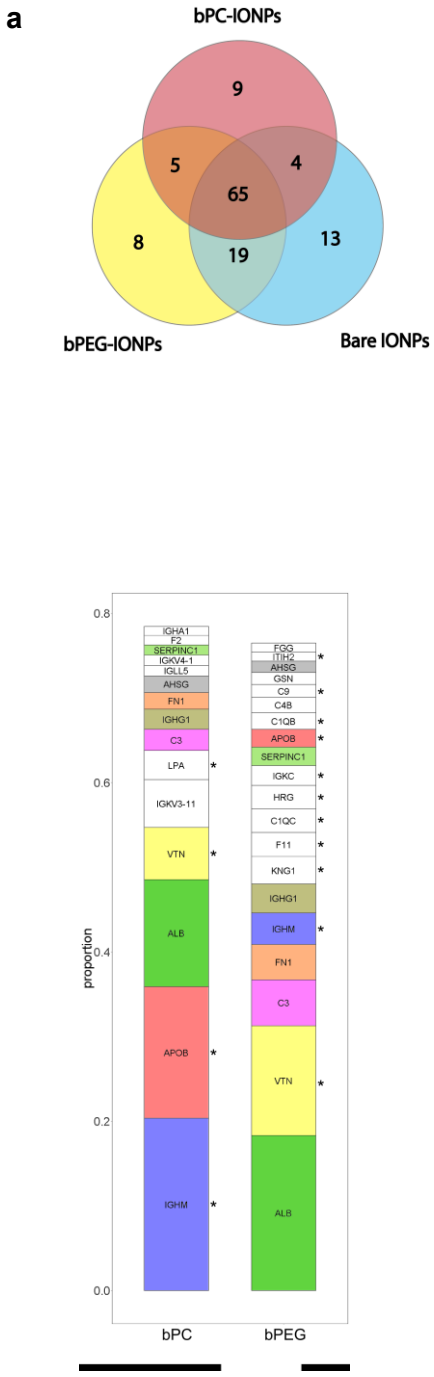

Figure 2. (a) Venn diagram representing the distribution of coronal proteins found to be associated with IONPs following incubation with human plasma. (b) Proportion comparison for those proteins contributing more than 1% of the total mean abundance for bPC and bPEG coronae. Asterisks indicate those proteins outside the 0.5 and 2.0 abundance ratio thresholds.

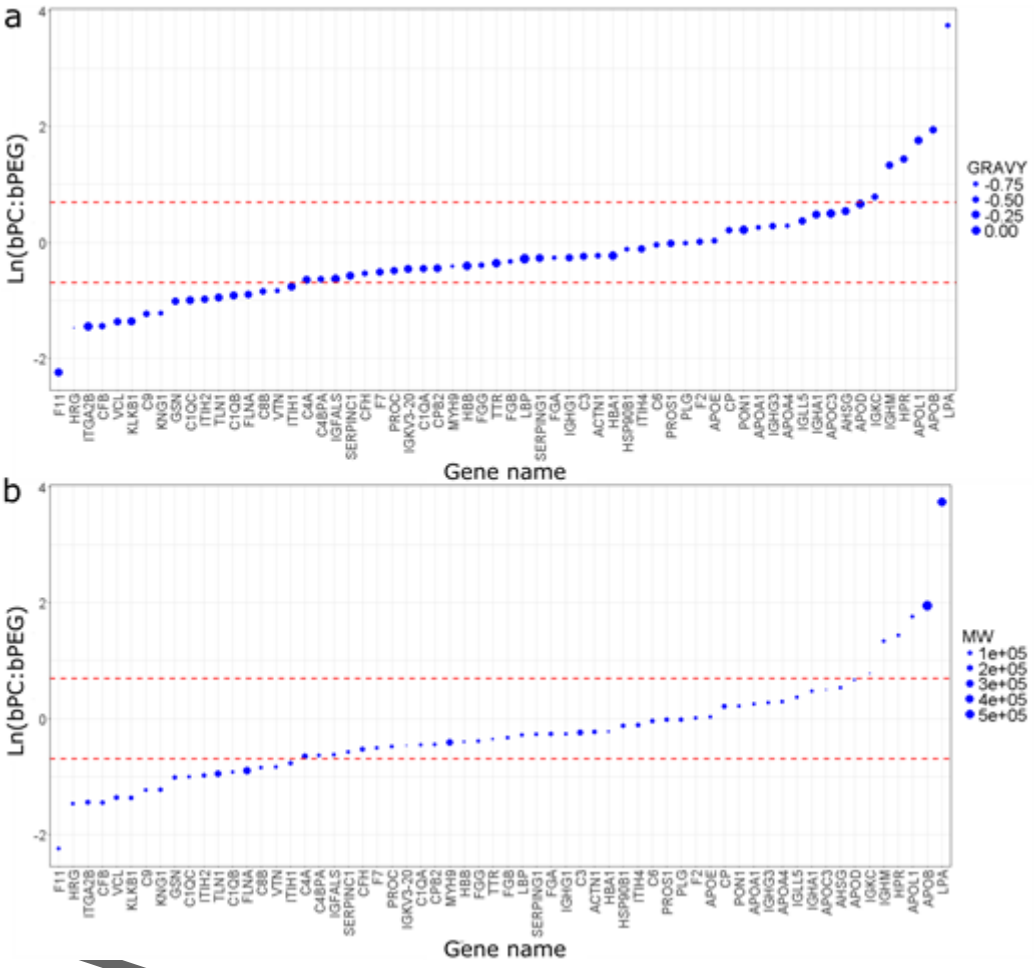

Figure 3. Log-normalized mean bPC:bPEG IONP protein corona abundances (red lines indicate Ln ratio cut-offs of 0.5 and 2.0). Gene names for each protein are sorted in ascending ratio value order based on ratio. (a) bPC:bPEG IONP abundance ratio with point size scaled to grand average of hydropathy (GRAVY) index. (b) bPC:bPEG IONP abundance ratio with point size scaled to molecular weight (MW). Plots generated in R and formatted in InkScape.

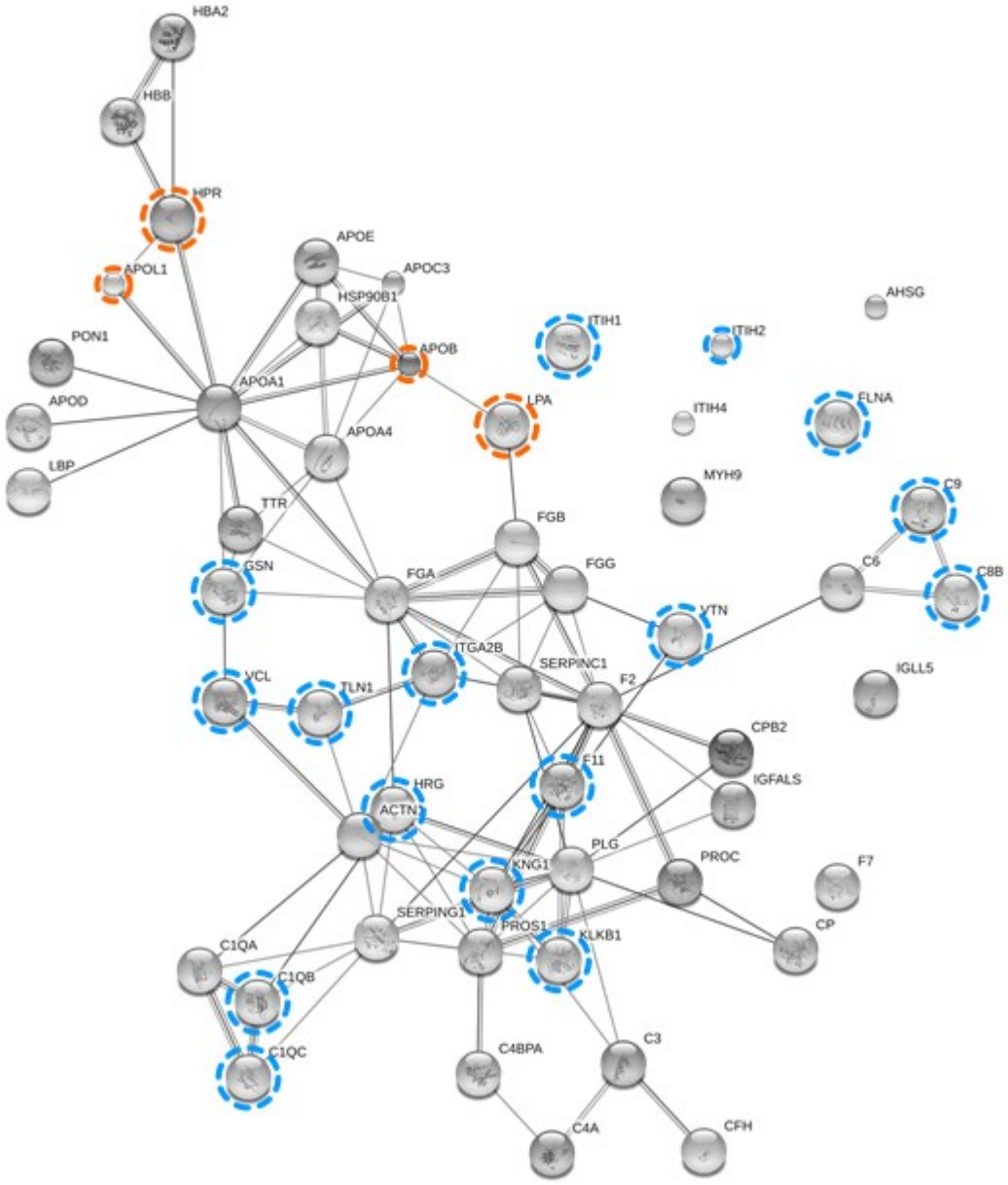

Figure 4. Protein network map across bPC and bPEG coronae. Proteins overrepresented in bPC versus bPEG coronae are outlined in orange, while proteins underrepresented are outlined in blue. Annotated network maps were generated using STRING (string-DB.org/) and formatted in InkScape.

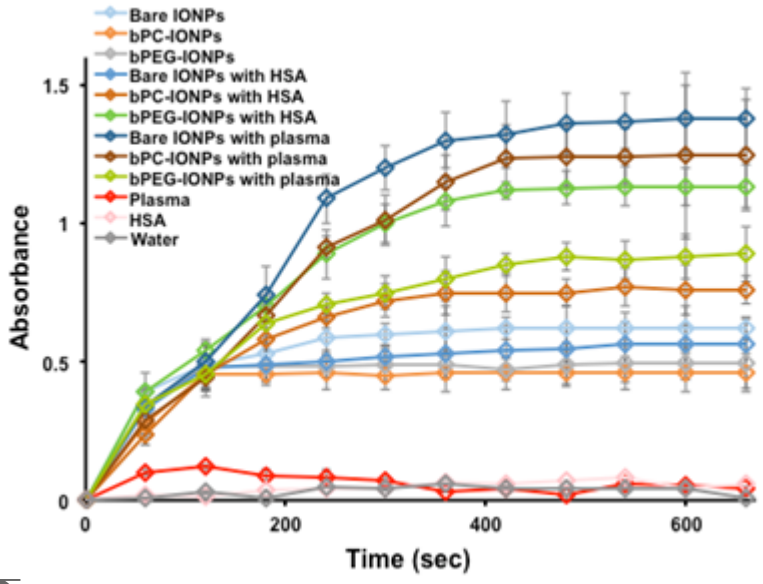

Figure 5. HRP-like activity of uncoated, HSA-coated, and plasma protein-coated bare, bPC and bPEG-IONPs.

TABLES

Table 1. Top 10 most abundant proteins associated with bare, bPC- and bPEG-IONPs and in plasma.

No.	Bare IONPs	bPC-IONPs	bPEG-IONPs	Plasma
1	Serum albumin	Ig heavy constant mu	Serum albumin	Serum albumin
2	Complement C3	Apolipoprotein B-100	Vitronectin	Ig heavy constant gamma 1
3	Vitronectin	Serum albumin	Complement C3	Fibrinogen beta chain
4	Ig heavy constant gamma 1	Vitronectin	Fibronectin	Complement C3
5	Coagulation factor XI	Ig kappa variable 3-11	Ig heavy constant mu	Serotransferrin
6	Kininogen-1	Apolipoprotein(a)	Ig heavy constant gamma 1	Apolipoprotein A-I
7	Complement C1q subcomponent subunit C	Complement C3	Kininogen-1	Alpha-1-antitrypsin
8	Apolipoprotein B-100	Ig heavy constant gamma 1	Coagulation factor XI	Fibrinogen alpha chain
9	Complement C4-A	Fibronectin	Complement C1q subcomponent subunit C	Haptoglobin
10	Ig kappa constant	Alpha-2-HS-glycoprotein	Histidine-rich glycoprotein	Alpha-2-macroglobulin

Table 2. Unique proteins to each IONP corona (bare, bPC and bPEG).

	Uniprot IDs	Protein names
bare IONPs	A0A087WZH9	Ig kappa variable 1D-33
	P01011	Alpha-1-antichymotrypsin
	P26038	Moesin
	O00391-2	Sulfhydryl oxidase 1
	P07357	Complement component C8 alpha chain
	Q13103	Secreted phosphoprotein 24
	E9PAQ1	Properdin
	P02749	Beta-2-glycoprotein 1
	B4DPQ0	Complement C1r subcomponent
	P00742	Coagulation factor X
	P01859	Ig gamma-2 chain C region
	P09871	Complement C1s subcomponent
	P02743	Serum amyloid P-component
bPC-IONPs	P11597	Cholesteryl ester transfer protein
	K7ER74	Apolipoprotein C-II
	P30101	Protein disulfide-isomerase A3
	P55058-3	Phospholipid transfer protein
	P01019	Angiotensinogen
	P01598	Ig kappa chain V-I region EU
	H3BM21	Integrin beta
	D6RD17	Immunoglobulin J chain
	K7ERI9	Apolipoprotein C-I
bPEG-IONPs	P08567	Pleckstrin
	P00488	Coagulation factor XIII A chain
	P63104	14-3-3 protein zeta/delta
	Q86UX7-2	Fermitin family homolog 3
	O43866	CD5 antigen-like
	A0A087WW89	Ig heavy variable 3-72
	P00738	Haptoglobin
	D6REX5	Selenoprotein P

Table 3. Protein abundance ratio of bPC-IONPs vs. bPEG-IONPs (less than 0.5 and greater than 2.0 was the fold difference threshold).

Uniprot IDs	Protein names (*Gene names*)	Mean ± SD	p value
P03951	Coagulation factor XI (*F11*)	0.11 ± 0.07	0.04
P04196	**Histidine-rich glycoprotein (*HRG*)**	**0.23 ± 0.11**	**0.02**
P08514	Integrin alpha-IIb (*ITGA2B*)	0.23 ± 0.16	0.04
P00751	**Complement factor B (*CFB*)**	**0.24 ± 0.15**	**0.04**
P18206	Vinculin (*VCL*)	0.25 ± 0.12	0.02
P03952	**Plasma kallikrein (*KLKB1*)**	**0.26 ± 0.13**	**0.02**
P02748	Complement component C9 (*C9*)	0.29 ± 0.09	0.01
P01042	**Kininogen-1 (*KNG1*)**	**0.29 ± 0.06**	**0.00**
P06396	Gelsolin (*GSN*)	0.36 ± 0.02	0.00
P02747	**Complement C1q subcomponent subunit C (*C1QC*)**	**0.37 ± 0.04**	**0.00**
P19823	Inter-alpha-trypsin inhibitor heavy chain H2 (*ITIH2*)	0.38 ± 0.12	0.01
Q9Y490	**Talin-1 (*TLN1*)**	**0.39 ± 0.06**	**0.00**
P02746	Complement C1q subcomponent subunit B (*C1QB*)	0.40 ± 0.04	0.00
P21333	**Filamin-A (*FLNA*)**	**0.41 ± 0.13**	**0.01**
P07358	Complement component C8 beta chain (*C8B*)	0.42 ± 0.29	0.04
P04004	**Vitronectin (*VTN*)**	**0.43 ± 0.11**	**0.00**
P19827	Inter-alpha-trypsin inhibitor heavy chain H1 (*ITIH1*)	0.46 ± 0.24	0.02
P01834	**Ig kappa constant (*IGKC*)**	**2.18 ± 0.40**	**0.00**
P01871	Ig heavy constant mu (*IGHM*)	3.81 ± 1.60	0.01
P00739	**Haptoglobin-related protein (*HPR*)**	**4.21 ± 2.34**	**0.02**
O14791	Apolipoprotein L1 (*APOL1*)	5.81 ± 3.12	0.02
P04114	**Apolipoprotein B-100 (*APOB*)**	**7.02 ± 4.37**	**0.03**
P08519	Apolipoprotein(a) (*LPA*)	41.99 ± 27.79	0.04

References

1. Cedervall, T.; Lynch, I.; Lindman, S.; Berggård, T.; Thulin, E.; Nilsson, H.; Dawson, K. A.; Linse, S. Understanding the Nanoparticle–Protein Corona Using Methods to Quantify Exchange Rates and Affinities of Proteins for Nanoparticles. *Proc. Natl. Acad. Sci. U.S.A.* **2007**, 104 (7), 2050-2055.

2. Lynch, I.; Dawson, K. A. Protein-Nanoparticle Interactions. *Nano Today* **2008**, 3 (1–2), 40-47.

3. Vroman, L.; Adams, A.; Fischer, G.; Munoz P. Interaction of High Molecular Weight Kininogen, Factor XII, and Fibrinogen in Plasma at Interfaces. *Blood* **1980**, 55 (1), 156-159.

4. Ding, F.; Radic, S.; Chen, R.; Chen, P.; Geitner, N. K.; Brown, J. M.; Ke, P. C. Direct Observation of A Single Nanoparticle-Ubiquitin Corona Formation. *Nanoscale* **2013**, 5 (19), 9162-9169.

5. Walkey, C. D.; Olsen, J. B.; Song, F.; Liu, R.; Guo, H.; Olsen, D. W. H.; Cohen, Y.; Emili, A.; Chan, W. C. W. Protein Corona Fingerprinting Predicts the Cellular Interaction of Gold and Silver Nanoparticles. *ACS Nano* **2014**, 8 (3), 2439-2455.

6. Palchetti, S.; Digiacomo, L.; Pozzi, D.; Peruzzi, G.; Micarelli, E.; Mahmoudi, M.; Caracciolo, G. Nanoparticles-Cell Association Predicted by Protein Corona Fingerprints. *Nanoscale* **2016**, 8 (25), 12755-12763.

7. Vogt, C.; Pernemalm, M.; Kohonen, P.; Laurent, S.; Hultenby, K.; Vahter, M.; Lehtiö, J.; Toprak, M. S.; Fadeel, B. Proteomics Analysis Reveals Distinct Corona Composition on Magnetic Nanoparticles with Different Surface Coatings: Implications for Interactions with Primary Human Macrophages. *PloS one* **2015**, 10 (10), e0129008.

8. Lundqvist, M.; Stigler, J.; Elia, G.; Lynch, I.; Cedervall, T.; Dawson, K. A. Nanoparticle Size and Surface Properties Determine the Protein Corona with Possible Implications for Biological Impacts. *Proc. Natl. Acad. Sci. U.S.A* **2008**, 105 (38), 14265-14270.

9. Hellstrand, E.; Lynch, I.; Andersson, A.; Drakenberg, T.; Dahlbäck, B.; Dawson, K. A.; Linse, S.; Cedervall, T. Complete High-Density Lipoproteins in Nanoparticle Corona. *FEBS Journal* **2009**, 276 (12), 3372-3381.

10. Salvati, A.; Pitek, A. S.; Monopoli, M. P.; Prapainop, K.; Bombelli, F. B.; Hristov, D. R.; Kelly, P. M.; Aberg, C.; Mahon, E.; Dawson, K. A. Transferrin-Functionalized Nanoparticles Lose Their Targeting Capabilities When A Biomolecule Corona Adsorbs on the Surface. *Nat. Nanotechnol.* **2013**, 8 (2), 137-143.

11. Arami, H.; Khandhar, A.; Liggitt, D.; Krishnan, K. M. In Vivo Delivery, Pharmacokinetics, Biodistribution and Toxicity of Iron Oxide Nanoparticles. *Chem. Soc. Rev*. **2015**, 44 (23), 8576-8607.

12. Malcolm, G. N.; Rowlinson, J. S. The Thermodynamic Properties of Aqueous Solutions of Polyethylene Glycol, Polypropylene Glycol and Dioxane. *Trans. Faraday. Soc*. **1957**, 53, 921-931.

13. Butcher, N. J.; Mortimer, G. M.; Minchin, R. F. Drug Delivery: Unravelling the Stealth Effect. *Nat. Nanotechnol*. **2016**, 11 (4), 310-311.

14. Furness, E. L.; Ross, A.; Davis, T. P.; King, G. C.; A Hydrophobic Interaction Site for Lysozyme Binding to Polyethylene Glycol and Model Contact Lens Polymers. *Biomaterials* **1998**, 19 (15), 1361-1369.

15. Brambilla, D.; Verpillot, R.; Le Droumaguet, B.; Nicolas, J.; Taverna, M.; Kóňa, J.; Lettiero, B.; Hashemi, S. H.; De Kimpe, L.; Canovi, M.; Gobbi, M.; Nicholas, V.; Scheper, W.; Moghimi, S. M.; Tvaroška, I.; Couvreur, P.; Andrieux, K. PEGylated Nanoparticles Bind to and Alter Amyloid-Beta Peptide Conformation: Toward Engineering of Functional Nanomedicines for Alzheimer's Disease. *ACS Nano* **2012**, 6 (7), 5897-5908.

16. Saha, K.; Rahimi, M.; Yazdani, M.; Kim, S. T.; Moyano, D. F.; Hou, S.; Das, R.; Mout, R.; Rezaee, F.; Mahmoudi, M.; Rotello, V. M. Regulation of Macrophage Recognition through the Interplay of Nanoparticle Surface Functionality and Protein Corona. *ACS Nano* **2016**, 10 (4), 4421-4430.

17. Schöttler, S.; Becker, G.; Winzen, S.; Steinbach, T.; Mohr, K.; Landfester, K.; Mailänder, V.; Wurm, F. R. Protein Adsorption Is Required for Stealth Effect of Poly(ethylene glycol)- and Poly(phosphoester)-Coated Nanocarriers. *Nat Nanotechnol*. **2016**, 11 (4), 372-377.

18. Garay, R. P.; El-Gewely, R.; Armstrong, J. K.; Garratty, G.; Richette, P. Antibodies against Polyethylene Glycol in Healthy Subjects and in Patients Treated with PEG-Conjugated Agents. *Expert Opin. Drug Deliv*. **2012**, 9 (11), 1319-1323.

19. Feng, W.; Brash, J. L.; Zhu, S. Non-Biofouling Materials Prepared by Atom Transfer Radical Polymerization Grafting of 2-Methacryloloxyethyl Phosphorylcholine: Separate Effects of Graft Density and Chain Length on Protein Repulsion. *Biomaterials* **2006**, 27 (6), 847-855.

20. Feng, W.; Gao, X.; McClung, G.; Zhu, S.; Ishihara, K.; Brash, J. L. Methacrylate Polymer Layers Bearing Poly(ethylene oxide) and Phosphorylcholine Side Chains as Non-Fouling Surfaces: In Vitro Interactions with Plasma Proteins and Platelets. *Acta Biomater*. **2011**, 7 (10), 3692-3699.

21. Matsuno, R.; Ishihara, K. Molecular-Integrated Phospholipid Polymer Nanoparticles with Highly Biofunctionality. *Macromol. Symp*. **2009**, 279 (1),125-131.

22. Müllner, M.; Cui, J.; Noi, K. F.; Gunawan, S. T.; Caruso, F. Surface-Initiated Polymerization within Mesoporous Silica Spheres for the Modular Design of Charge-Neutral Polymer Particles. *Langmuir* **2014**, 30 (21), 6286-6293.

23. Blin, T.; Kakinen, A.; Pilkington, E. H.; Ivask, A.; Ding, F.; Quinn, J. F. Whittaker, M. R.; Ke, P. C.; Davis, T. P. Synthesis and In Vitro Properties of Iron Oxide Nanoparticles Grafted With Brushed Phosphorylcholine and Polyethylene Glycol. *Polym. Chem*. **2016**, 7 (10),1931-1944.

24. Wang, B.; Blin, T.; Kakinen, A.; Ge, X.; Pilkington, E. H.; Quinn, J. F.; Whittaker, M. R.; Davis, T. P.; Ke, P. C.; Ding, F. Brushed Polyethylene Glycol and Phosphorylcholine for Grafting Nanoparticles against Protein Binding. *Polym. Chem*. **2016**, 7 (45), 6875-6879.

25. Shannahan, J. H.; Brown, J. M.; Chen, R.; Ke, P. C.; Lai, X.; Mitra, S.; Witzmann, F. A. Comparison of Nanotube–Protein Corona Composition in Cell Culture Media. *Small* **2013**, 9 (12), 2171-2181.

26. Shannahan, J. H.; Lai, X.; Ke, P. C.; Podila, R.; Brown, J. M.; Witzmann, F. A. Silver Nanoparticle Protein Corona Composition in Cell Culture Media. *PloS one* **2013**, 8 (9), e74001.

27. Simberg, D.; Park, J-H.; Karmali, P. P.; Zhang, W-M.; Merkulov, S.; McCrae, K.; Bhatia, S. N.; Sailor, M.; Ruoslahti, E. Differential Proteomics Analysis of the Surface Heterogeneity of

Dextran Iron Oxide Nanoparticles and the Implications for Their In Vivo Clearance. *Biomaterials* **2009**, 30 (23–24), 3926-3933.

28. Veiseh, O.; Gunn, J. W.; Zhang, M. Design and Fabrication of Magnetic Nanoparticles for Targeted Drug Delivery and Imaging. *Adv. Drug Deliv. Rev*. **2010**, 62 (3), 284-304.

29. Basuki, J. S.; Esser, L.; Duong, H. T. T.; Zhang, Q.; Wilson, P.; Whittaker, M. R.; Haddleton, D. M.; Boyer, C.; Davis, T. P. Magnetic Nanoparticles with Diblock Glycopolymer Shells Give Lectin Concentration-Dependent MRI Signals and Selective Cell Uptake. *Chem. Sci*. **2014**, 5 (2), 715-726.

30. Basuki, J. S.; Duong, H. T. T.; Macmillan, A.; Erlich, R. B.; Esser, L.; Akerfeldt, M. C.; Whan, R. M.; Kavallaris, M.; Boyer, C.; Davis, T. P. Using Fluorescence Lifetime Imaging Microscopy to Monitor Theranostic Nanoparticle Uptake and Intracellular Doxorubicin Release. *ACS Nano* **2013**, 7 (11), 10175-10189.

31. Nguyen, T. T. T.; Duong, H. T. T.; Basuki, J.; Montembault, V.; Pascual, S.; Guibert, C.; Fresnais, J.; Boyer, C.; Whittaker, M. R.; Davis, T. P.; Fontaine, L. Functional Iron Oxide Magnetic Nanoparticles with Hyperthermia-Induced Drug Release Ability by Using a Combination of Orthogonal Click Reactions. *Angew. Chem. Int. Ed*. **2013**, 125 (52), 14402-14406.

32. Laurent, S.; Mahmoudi, M. Superparamagnetic Iron Oxide Nanoparticles: Promises for Diagnosis and Treatment of Cancer. *Int. J. Mol. Epidemiol. Genet*. **2011**, 2 (4), 367-390.

33. Gao, L.; Zhuang, J.; Nie, L.; Zhang, J.; Zhang, Y.; Gu, N.; Wang, T.; Feng, J.; Yang, D.; Perrett, S.; Yan, X. Intrinsic Peroxidase-Like Activity of Ferromagnetic Nanoparticles. *Nat. Nanotechnol*. **2007**, 2 (9), 577-583.

34. Yu, F.; Huang, Y.; Cole, A. J.; Yang, V. C. The Artificial Peroxidase Activity of Magnetic Iron Oxide Nanoparticles and its Application to Glucose Detection. *Biomaterials* **2009**, 30 (27), 4716-4722.

35. Boyer, C.; Whittaker, M. R.; Bulmus, V.; Liu, J.; Davis, T. P. The Design and Utility of Polymer-Stabilized Iron-Oxide Nanoparticles for Nanomedicine Applications. *NPG Asia Mater*. **2010**, 2, 23-30.

36. Boyer, C.; Priyanto, P.; Davis, T. P.; Pissuwan, D.; Bulmus, V.; Kavallaris, M.; Teoh, W. Y.; Amal, R.; Carroll, M.; Woodward, R.; St Pierre. T. Anti-Fouling Magnetic Nanoparticles for siRNA Delivery. *J. Mater. Chem*. **2010**, 20 (2), 255-265.

37. Boyer, C.; Bulmus, V.; Priyanto, P.; Teoh, W. Y.; Amal, R.; Davis, T. P. The Stabilization and Bio-Functionalization of Iron Oxide Nanoparticles Using Heterotelechelic Polymers. *J. Mater. Chem*. **2009**, 19 (1), 111-123.

38. Liu, G.; Zhao, Y.; Angeles, A.; Hamuro, L. L.; Arnold, M. E.; Shen, J. X. A Novel and Cost Effective Method of Removing Excess Albumin from Plasma/Serum Samples and Its Impacts on LC-MS/MS Bioanalysis of Therapeutic Proteins. *Anal. Chem*. **2014**, 86 (16), 8336-8343.

39. Rappsilber, J.; Ishihama, Y.; Mann, M. Stop and Go Extraction Tips for Matrix-Assisted Laser Desorption/ Ionization, Nanoelectrospray, and LC/MS Sample Pretreatment in Proteomics. *Anal. Chem*. **2003**, 75 (3), 663-670.

40. Siddiqui, G.; Srivastava, A.; Russell, A. S.; Creek, D. J. Multi-Omics Based Identification of Specific Biochemical Changes Associated with PfKelch13-Mutant Artemisinin Resistant Plasmodium Falciparum. *J. Infect. Dis*. **2017**, doi: 10.1093/infdis/jix156.

41. Cox, J.; Mann, M. MaxQuant Enables High Peptide Identification Rates, Individualized p.p.b.-Range Mass Accuracies and Proteome-Wide Protein Quantification. *Nat. Biotech.* **2008**, 26 (12), 1367-1372.

42. Cox, J.; Neuhauser, N.; Michalski, A.; Scheltema, R. A.; Olsen, J. V.; Mann M. Andromeda: A Peptide Search Engine Integrated into the MaxQuant Environment. *J. Proteome Res*. **2011**, 10 (4), 1794-1805.

43. Hubner, N. C.; Bird, A. W.; Cox, J.; Splettstoesser, B.; Bandilla, P.; Poser, I.; Hyman, A.; Mann, M. Quantitative Proteomics Combined with BAC Transgene Omics Reveals In Vivo Protein Interactions. *J. Cell Biol*. **2010**, 189 (4), 739-754.

44. Szklarczyk, D.; Franceschini, A.; Wyder, S.; Forslund, K.; Heller, D.; Huerta-Cepas, J.; Simonovic, M.; Roth, A.; Santos, A.; Tsafou, K. P.; Kuhn, M.; Bork, P.; Jensen, L. J.; von Mering, C. STRING v10: Protein-Protein Interaction Networks, Integrated over the Tree of Life. *Nucleic Acids Res*. **2015**, 43 (Database issue), D447-D452.

45. Docter, D.; Distler, U.; Storck, W.; Kuharev, J.; Wünsch, D.; Hahlbrock, A.; Knauer, S. K.; Tenzer, S.; Stauber, R. H. Quantitative Profiling of the Protein Coronas that Form Around Nanoparticles. *Nat. Protoc*. **2014**, 9 (9), 2030-2044.

46. Farrah, T.; Deutsch, E. W.; Omenn, G. S.; Campbell, D. S.; Sun, Z.; Bletz, J. A.; Mallick, P.; Katz, J. E.; Malmström, J.; Ossola, R.; Watts, J. D.; Lin, B.; Zhang, H.; Moritz, R. L.; Aebersold, R. A High-Confidence Human Plasma Proteome Reference Set with Estimated Concentrations in PeptideAtlas. *Mol. Cell Proteomics* **2011**, 10 (9), 110-006353

47. Tenzer, S.; Docter, D.; Rosfa, S.; Wlodarski, A.; Kuharev, J.; Rekik, A.; Knauer, S. K.; Bantz, C.; Nawroth, T.; Bier, C.; Sirirattanapan, J.; Mann, W.; Treuel, L.; Zellner, R.; Maskos, M.; Schild, H.; Stauber, R. H. Nanoparticle Size Is a Critical Physicochemical Determinant of the Human Blood Plasma Corona: A Comprehensive Quantitative Proteomic Analysis. *ACS Nano* **2011**, 5 (9), 7155-7167.

48. Dobrovolskaia, M. A.; Aggarwal, P.; Hall, J. B.; McNeil, S. E. Preclinical Studies To Understand Nanoparticle Interaction with the Immune System and Its Potential Effects on Nanoparticle Biodistribution. *Mol. Pharm*. **2008**, 5 (4), 487-495.

49. Pelaz, B.; del Pino, P.; Maffre, P.; Hartmann, R.; Gallego, M.; Rivera-Fernández, S.; de la Fuente, J. M.; Nienhaus, G. U.; Parak, W. J. Surface Functionalization of Nanoparticles with Polyethylene Glycol: Effects on Protein Adsorption and Cellular Uptake. *ACS Nano* **2015**, 9 (7), 6996-7008.

50. Albanese, A.; Walkey, C. D.; Olsen, J. B.; Guo, H.; Emili, A.; Chan, W. C. W. Secreted Biomolecules Alter the Biological Identity and Cellular Interactions of Nanoparticles. *ACS Nano* **2014**, 8 (6), 5515-5526.

51. Walkey, C. D.; Olsen, J. B.; Guo, H.; Emili, A.; Chan, W. C. W. Nanoparticle Size and Surface Chemistry Determine Serum Protein Adsorption and Macrophage Uptake. *J. Am. Chem. Soc*. **2012**, 134 (4), 2139-2147.

52. Zhang, H. L.; Zou, X. Z.; Lai, G. S.; Han, D. Y.; Wang, F. Direct Electrochemistry of Hemoglobin Immobilized on Carbon-Coated Iron Nanoparticles for Amperometric Detection of Hydrogen Peroxide. *Electroanalysis* **2007**, 19 (18), 1869-1874.

53. Xiao, J.; Zhao, Y.; Wang, H.; Yuan, Y.; Yang, F.; Zhang, C.; Yamamoto, K. Noncovalent Interaction of Dietary Polyphenols with Common Human Plasma Proteins. *J. Agric. Food Chem*. **2011**, 59 (19), 10747-10754.

Table of Content

Recent research has revealed adverse effects following the administration of PEG, prompting this study of plasma protein association with iron oxide nanoparticles (IONPs) grafted with brushed PEG and phosphorylcholine. Our observations support the rational design of stealth polymers based on understanding the interplay between IONPs and the plasma proteome, and should prove beneficial for the development of nanomedicine and catalysis.

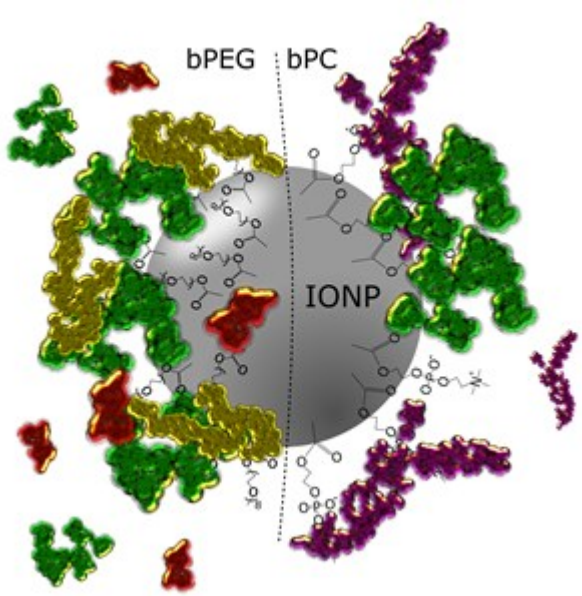

Author/s:
Wang, M; Siddiqui, G; Gustafsson, OJR; Kakinen, A; Javed, I; Voelcker, NH; Creek, DJ; Ke, PC; Davis, TP

Title:
Plasma Proteome Association and Catalytic Activity of Stealth Polymer-Grafted Iron Oxide Nanoparticles

Date:
2017-09-27

Citation:
Wang, M., Siddiqui, G., Gustafsson, O. J. R., Kakinen, A., Javed, I., Voelcker, N. H., Creek, D. J., Ke, P. C. & Davis, T. P. (2017). Plasma Proteome Association and Catalytic Activity of Stealth Polymer-Grafted Iron Oxide Nanoparticles. SMALL, 13 (36), https://doi.org/10.1002/smll.201701528.